

Vibration and Tracking Control of a Flexure-Guided Nanopositioner Using a Piezoelectric Strain Sensor

Y. K. Yong, A. J. Fleming and S. O. R. Moheimani
School of Electrical Engineering and Computer Science,
The University of Newcastle, Callaghan 2308, NSW Australia.
yuenkuan.yong@newcastle.edu.au

Abstract—This paper presents a novel sensing technique which uses a piezoelectric strain sensor for damping and accurate tracking of a nanopositioning stage. Piezoelectric elements have been used effectively as sensors for vibration control of smart structures. However, complications arise when one uses a piezoelectric strain sensor in a feedback loop for tracking. This is due to the high-pass characteristic of the piezoelectric strain voltage at low frequencies which tends to destabilize a closed-loop tracking system. Here, we overcome this problem by using a low-frequency bypass technique which replaces the low frequency signal with an estimate based on the open-loop system. Once the high-pass characteristic is accounted for, an analog Integral Resonant Control (IRC) and an integral tracking controller were implemented. The resultant tracking bandwidth of the closed-loop system was measured to be 1.86 kHz. To evaluate the closed-loop tracking performance of the nanopositioning stage, it was forced to track triangular waveforms at 40 Hz and 78 Hz. The closed-loop system shows significant improvement where the non-linearity of the system is effectively reduced.

I. INTRODUCTION

The Atomic Force Microscope (AFM) is an important tool in the area of nanotechnology including bioscience [1], electrical characterization of semiconductors [2], nanomanipulation and nanoassembly [3]. In an AFM, a sample is placed on a piezoelectric tube scanner [4]. A sharp probe located at the free end of a micro-cantilever is used to measure the sample topography. The scanner moves the sample in a raster pattern over an area. The topographical image is then generated by recording the interaction between the probe and sample as a function of position.

Flexure-based, piezoelectric stack-actuated nanopositioners have emerged as an alternative scanner for high-speed atomic force microscopy [5]–[9]. The two main drawbacks of flexure-based mechanisms are (i) the lightly damped resonant peaks, and (ii) the non-linearity of piezoelectric stack actuators. A triangular waveform that is used to generate the raster pattern tends to excite the resonant peaks of a nanopositioner which in turn distorts the AFM images. The piezoelectric non-linearity causes positioning errors which induces image artifacts. Various feedback control techniques have been successfully implemented to suppress vibration and to compensate for positioning errors [7], [10], [11]. These feedback control methods use position sensors such as capacitive and inductive sensors, which typically have a maximum bandwidth of 10 kHz. The first resonant peak of most high-speed nanopositioners appear at above 10 kHz [5]–[7]. These sensors are clearly inadequate

for high-bandwidth closed-loop control of nanopositioners. Furthermore, these sensors are typically expensive and large in size, making the installation of the sensors to a compact nanopositioner rather difficult.

In this work, a piezoelectric strain sensor is used as a position sensor in a feedback loop to damp the first resonant peak and to provide accurate tracking of a nanopositioner. Piezoelectric elements are small and compact which can be easily bonded to flexures to measure displacements. Piezoelectric strain sensors provide a high sensitivity and bandwidth with low noise at high frequencies [12], [13]. This property is desirable for high-speed nanopositioning applications. Piezoelectric elements have been used effectively as sensors for vibration control of smart structures [14]–[19]. Unfortunately, there are difficulties in closed-loop tracking control due to the high-pass characteristic of piezoelectric strain voltage at low frequencies. This high-pass characteristic is due to the piezoelectric capacitance and finite input impedance of voltage amplifiers and buffers.

In this work, the high-pass characteristic problem is solved by implementing a low-frequency bypass technique where the low frequency signal is replaced with an estimate signal based on the open-loop system dynamics [13]. The low-frequency bypass technique facilitates the implementation of an integral tracking controller.

It is documented in Ref. [13] that by suppressing the lightly damped resonance of a system, the bandwidth of an integral tracking controller can be significantly increased. Therefore, an Integral Resonant Control (IRC) [20], [21] was implemented together with an integral tracking controller to achieve a high resultant tracking bandwidth of the nanopositioner.

The remainder of the paper is organized as follows. A description of the experimental setup is provided in Sec. II. In Sec. III, the characteristic of piezoelectric strain sensor is discussed. The relationship between mechanical strain and voltage of the piezoelectric sensor is also derived analytically. The feedback control design is then discussed in Sec. IV followed by the open- and closed-loop performances of the nanopositioning stage in Sec. V. Sec. VI concludes the paper.

II. EXPERIMENTAL SETUP

The proposed sensing technique will be demonstrated on the fast-scanning axis (i.e. Y-axis) of an XYZ flexure-based nanopositioner. As pictured in Fig. 1. The X- and Y-axis of

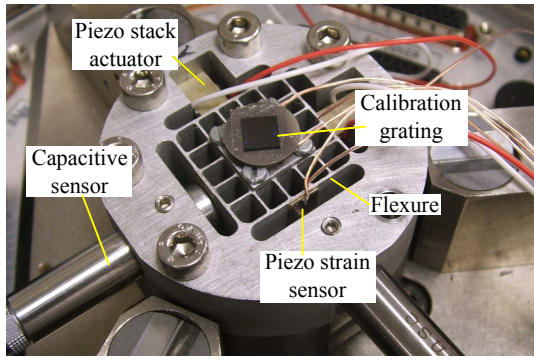


Figure 1. A XYZ nanopositioner with piezoelectric strain sensor.

the nanopositioner are driven by Noliac SCMAP07 piezoelectric stack actuators (5 mm × 5 mm × 10 mm, 380 nF). The Z-axis is driven by a Noliac SCMAP06 stack actuator (3 mm × 3 mm × 6 mm, 70 nF). The nanopositioner has a motion range of 7 μm × 7 μm × 4 μm in the X-, Y- and Z-axis respectively. The first resonance frequency of the three axes is 11.3 kHz.

The piezoelectric strain sensor is a 5 mm × 10 mm × 0.25 mm plate of PI PIC151 piezoelectric ceramic bonded to the flexure with epoxy as shown in Fig. 1. The induced piezoelectric voltage was buffered by a unity-gain amplifier with an input impedance of 500 MΩ. Due to the 4-nF source capacitance of the sensor, the resulting high-pass cut-off frequency was 0.1 Hz. In order to calibrate the piezoelectric sensor, a MicroSense 6810 capacitive sensor with a sensitivity of 2.5 μm/V was also used to measure the displacement of the nanopositioner.

The Y-axis piezoelectric actuator was driven by a charge-drive with a gain of 10 μC/V and an equivalent voltage gain of 26. All frequency responses were recorded using a HP35670A dual-channel spectrum analyzer. To evaluate the closed-loop tracking performance, the nanopositioner was forced to track fast triangular waveforms at 40 Hz and 78 Hz.

III. PIEZOELECTRIC STRAIN SENSOR

To measure the dynamic deflection of the nanopositioner, a piezoelectric plate is bonded to the flexure as shown in Fig. 2. Since the deflection is proportional to strain, the induced piezoelectric voltage is also proportional to deflection. This relationship is explored in the following.

If the piezoelectric actuator is modeled as a center-located point-load, the transverse deflection $y(x)$ of a fixed-fixed uniform beam is known to be [22]

$$y(x) = \frac{F}{24EI} \left(2x^3 - \frac{3}{2}lx^2 \right) \text{ for } 0 < x < \frac{l}{2}, \quad (1)$$

where F is the applied force, E is the Young's Modulus, and I is the moment of inertia. Although the above equation describes only one half of the beam deflection, the deflection is symmetric about the mid-point. If the deflection d at the

mid-point is known, Eq. (1) can be simplified to:

$$y(x) = -d \frac{8}{l^3} \left(2x^3 - \frac{3}{2}lx^2 \right) \text{ for } 0 < x < \frac{l}{2}, \quad (2)$$

Once the deflection is known, the induced piezoelectric voltage can be derived. Since the sensor is thin compared to the host structure, the strain S_1 in the sensor is assumed to be uniform through its thickness. That is,

$$S_1 = -cy''(x), \quad (3)$$

where c is the distance to the neutral axis. The induced voltage v_p can be shown to be [23]

$$v_p = K \frac{d_{31} E_p w_p}{C_p} \int S_1 dx, \quad (4)$$

where K is a correction factor, E_p is the Young's Modulus of the piezoelectric material, w_p is the sensor width, d_{31} is the strain-charge coupling coefficient, and C_p is the capacitance given by $C_p = \frac{l_p w_p \epsilon_{33}}{t_p}$, where t_p is the piezo thickness, l_p is the piezo length, and ϵ_{33} is the dielectric permittivity under constant stress. The correction factor $K = K_p K_b$ accounts for the lateral strain due to poisson coupling and the shear-lag effect of the bonding layer [23]. Sensors constructed from PZT are equally sensitive to lateral and longitudinal strain, so $K_p = (1 - \nu)$ where ν is the poisson ratio for aluminium (0.33) [23]. The shear-lag factor K_b is caused by the bonding layer which reduces the strain experienced by the sensor. By assuming a bond layer thickness of 0.028 mm, the effective length and width fractions of the proposed sensor are 0.6783 and 0.8385 respectively. The equivalent area factor is $K_b = 0.6783 \times 0.8385 = 0.5688$.

Since the deflection is symmetrical about the midpoint, the derivation of induced voltage can be simplified by considering a piezoelectric sensor that covers only one half of the beam; that is, the length l_p is halved. Due to the symmetry about the midpoint, the induced voltage on the full sensor is equal to the half-sensor but with twice the capacitance. Taking this into account and combining Eqs. (2) and (4) yields

$$v_p = K \frac{d_{31} E_p w_p}{C_p/2} cd \frac{8}{l^3} [y'(x)]_{\frac{l}{2} - \frac{l_p}{2}}^{\frac{l}{2}} \quad (5)$$

$$v_p = K \frac{d_{31} E_p w_p}{C_p/2} cd \frac{8}{l^3} [6x^2 - 3lx]_{\frac{l}{2} - \frac{l_p}{2}}^{\frac{l}{2}}, \quad (6)$$

$$v_p = K \frac{d_{31} E_p w_p}{C_p/2} cd \frac{8}{l^3} \left(\frac{3ll_p}{2} - \frac{3l_p^2}{2} \right). \quad (7)$$

Eq. (7) demonstrates that the induced voltage is linearly proportional to the deflection of the nanopositioner. The parameters of the piezoelectric strain sensor and the flexure dimensions are listed in Table I.

From Eq. (7) and Table I, the estimated sensitivity is 1.3 V/μm of deflection at the mid-point. The experimentally measured sensitivity was 1.06 V/μm, which is lower than the predicted value. The discrepancy is thought to be due to the lower curvature caused by the 5-mm wide piezoelectric actuator, which locally stiffens the structure and acts as a distributed force not the assumed point load.

Table I
PROPERTIES OF THE PIEZOELECTRIC STRAIN SENSOR AND THE FLEXURE DIMENSIONS.

E_p GPa	d_{31} C/N	C_p nF	l_p mm	t_p mm	w_p mm
66	-210×10^{-12}	4.25	5	0.25	10

l mm	t mm	w mm	c mm
16	0.4	12.8	0.325

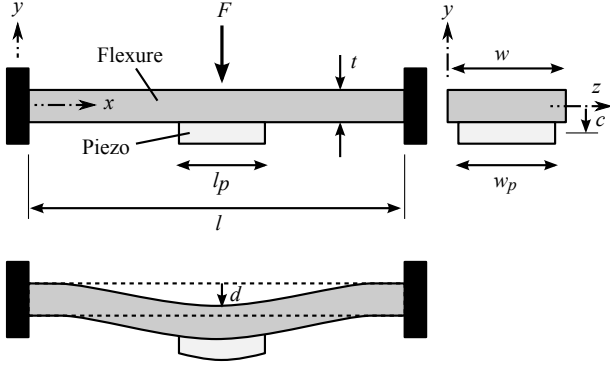


Figure 2. Schematic diagram of a flexure with a bonded piezoelectric plate.

A. Sensor characteristics

Due to the capacitive nature of the piezoelectric sensor and the finite input impedance of electronics, the transfer function from v_p to \widehat{V}_s resembles a first-order high-pass filter H_p [13], that is

$$V_s = H_p(s) v_p, \quad \text{where } H_p(s) = \frac{s}{s + \omega_c}, \quad (8)$$

v_p is the piezoelectric strain voltage, and $\omega_c = 1/R_{in}C_p$, where R_{in} is the input impedance of the voltage buffer and C_p is the piezoelectric sensor capacitance. This high-pass characteristic causes a standard tracking controller to saturate.

To evaluate the sensor characteristics at dynamic frequencies, the frequency response functions (FRFs) of the nanopositioning system were recorded from the input applied to the charge amplifier to (i) the measured strain voltage $G_{vv}(i\omega)$ and (ii) the measured displacement $G_{dv}(i\omega)$. Note that d is the displacement of the nanopositioner measured using a capacitive sensor. The two FRFs are plotted in Fig. 4. The first resonant peak of the system appears at 11.3 kHz in both plots.

To evaluate the linearity of the piezoelectric strain sensor, a 100-Hz triangular input signal of 200 V was applied to the actuator. In Fig. 3, the measured capacitive sensor signal is identical to the piezoelectric strain sensor signal to within the limits of measurement.

IV. MODELING, CONTROLLER DESIGN AND IMPLEMENTATION

To facilitate the controller design, a dynamic model is first required for the system. The nanopositioning system is considered to be a single-input two-output (SITO) system

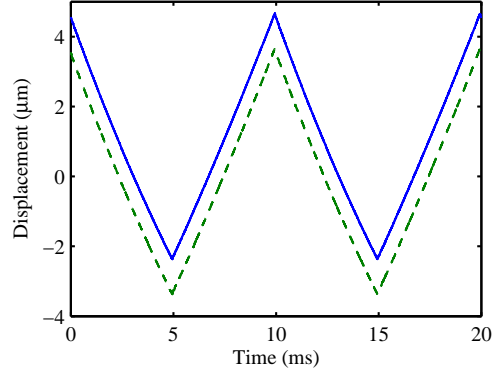


Figure 3. The measured displacement in response to a full-range 100-Hz triangle wave (200 V). The solid line is the displacement measurement derived from the piezoelectric strain sensor \widehat{V}_s (-) while the dashed line is from the capacitive sensor d (-). V_s is plotted with a 1 μm positive offset for the sake of clarity.

where the input is applied voltage V_a and the outputs are displacement d and the piezoelectric strain voltage v_p . This SITO system is expressed as

$$\begin{bmatrix} d \\ v_p \end{bmatrix} = G(s) u, \quad \text{and} \quad G(s) = \begin{bmatrix} G_{dv}(s) \\ G_{vv}(s) \end{bmatrix}. \quad (9)$$

A second-order model was fitted to the measured frequency responses in Fig. 4 using the frequency domain subspace algorithm [24]. The transfer functions of the two subsystems are

$$G_{vv}(s) = \frac{0.1662s^2 - 8569s + 2.684 \times 10^9}{s^2 + 5480s + 5.226 \times 10^9}, \quad (10)$$

$$G_{dv}(s) = \frac{0.01825s^2 - 7453s + 1.105 \times 10^9}{s^2 + 5480s + 5.226 \times 10^9}. \quad (11)$$

The measured and modeled frequency responses of G_{vv} and G_{dv} are plotted in Fig. 4.

A. Damping control

It is known that the bandwidth and stability margins of a standard tracking control system are proportional to the magnitude of the lowest-frequency resonance peak [25]. Hence, in order to maximize the closed-loop bandwidth of the nanopositioner, an Integral Resonance Controller (IRC) was designed to damp the first resonance mode. A block diagram of the system with IRC damping control is illustrated in Fig. 5. The shaded box in Fig. 5 represents the damped system $\widehat{G}(s)$.

The IRC damping controller was designed by following the procedure in Ref. [20]. This procedure begins by finding a sufficiently large feedthrough term D_f so that the system zeros are lower than the resonance frequency. The new system with added feed-through is referred to as $G_{vv}(s) + D_f$. A suitable gain k can then be found using the root-locus technique [25]. In this case, $D_f = -1$ and $k = 7 \times 10^4$ were used.

Due to the high mechanical resonance mode (11.3 kHz) and the limited sampling rate of the dSPACE prototyping system, the IRC controller was implemented in analog form

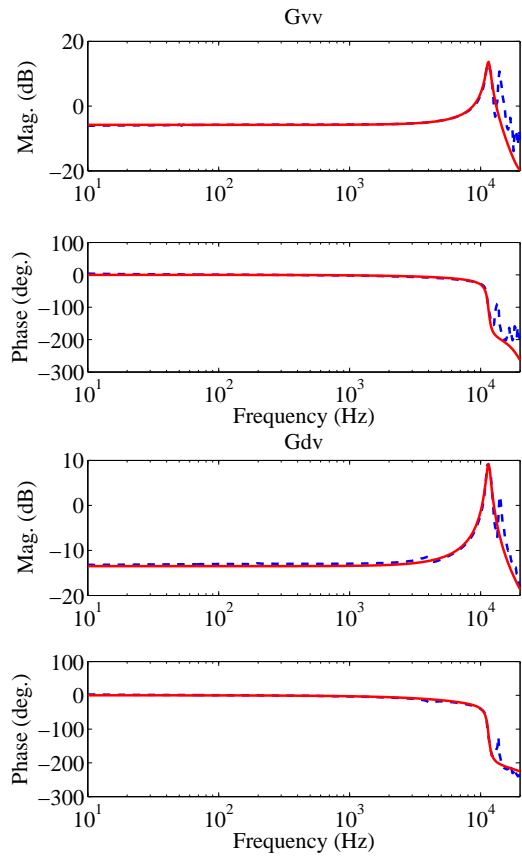


Figure 4. Measured (—) and modeled (---) frequency responses of G_{vv} and G_{dv} .

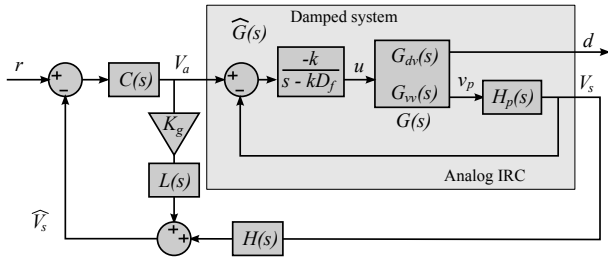


Figure 5. Block diagram of the damped system $\hat{G}(s)$ using the IRC and the low-frequency bypass control technique.

[25]. Although the transfer function can be implemented by a single op-amp, the dual configuration, shown in Fig. 6, is simpler to tune if necessary.

The first stage of the circuit in Fig. 6 is a unity-gain differential amplifier. The controller IRC controller is implemented by the inverting integrator stage C_2 , where

$$C_2 = \frac{-k}{s - kD_f}. \quad (12)$$

The circuit transfer function is

$$\frac{-\frac{1}{r_{2a}c_2}}{s + \frac{1}{r_{2b}c_2}}. \quad (13)$$

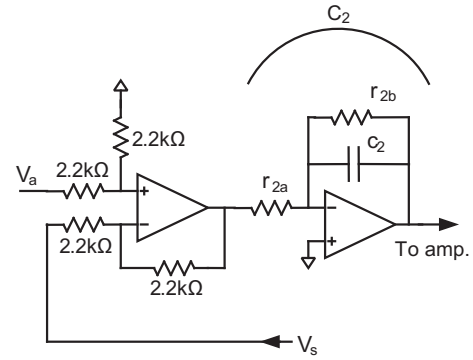


Figure 6. Analog implementation of the IRC damping controller.

As k is positive and D_f is negative, the equalities are

$$r_{2a}c_2 = \frac{1}{k}, \text{ and } r_{2b}c_2 = \frac{1}{kD_f}. \quad (14)$$

The component values used to implement the controller are listed below. The opamp is an LT1362, however almost any general purpose high-speed opamp would be suitable.

r_{2a}	r_{2b}	c_2
4.33 kΩ	4.33 kΩ	3.3 nF

B. Tracking control

As discussed in Sec. III-A, the high-pass characteristic of the piezoelectric strain voltage precludes the direct use of an integral tracking controller. In this work, we use the low-frequency bypass technique [13] that allows the piezoelectric strain voltage to be used for tracking. In this technique, the complementary filters $L(s)$ and $H(s)$ (see Fig. 5) are used to substitute the actual output with an estimate at frequencies below the crossover frequency α , chosen to be 10 Hz. The transfer functions of the complementary filters are

$$H(s) = \frac{\alpha}{(s + \alpha)}, \text{ and } L(s) = 1 - H_p(s)H(s) \quad (15)$$

where $H_p(s)$ is the high-pass filter associated with the piezoelectric strain voltage defined in Eq. (8) that has a cut-off frequency of 0.1 Hz. The signal V_a is scaled to have the same sensitivity as V_s by a constant K_g . Providing K_g is accurately tuned, the transfer function from r to V_s is

$$\frac{V_s}{r} = \frac{C(s)\hat{G}_{vv}(s)}{1 + C(s)(K_gL(s) + \hat{G}_{vv}(s)H(s))}, \quad (16)$$

where $C(s)$ is a negative integral controller, $C(s) = -k_i/s$. The transfer function from r to d is

$$\frac{d}{r} = \frac{C(s)\hat{G}_{dv}(s)}{1 + C(s)(K_gL(s) + \hat{G}_{vv}(s)H(s))}. \quad (17)$$

Piezoelectric stack actuators exhibit significant hysteresis when driven with large voltages. This can cause the system sensitivity and K_g to be dependent on the voltage magnitude. However, in this work a charge drive [26] was used to effectively eliminate hysteresis. K_g was successfully tuned to

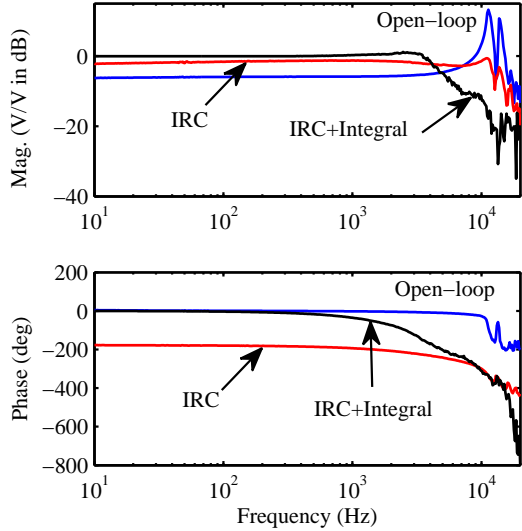


Figure 7. Measured frequency responses of the open-loop system, the damped system with IRC and the closed-loop system with IRC and integral tracking control.

-1.05. An alternative method to account for the presence of hysteresis involves the inclusion of a non-linear model in K_g . The Preisach model [27], Prandtl-Ishlinskii operator [28] and Maxwell resistive capacitor model [29] have all been used to effectively model low-frequency hysteresis.

The experimental frequency responses of the open-loop, damped, and closed-loop system are plotted in Fig. 7. The resulting tracking bandwidth of the closed-loop system is 1.86 kHz (45° phase lag) when using an integral gain of $k_i = 15000$. The gain and phase margins are 11.3 dB and 58.6° respectively. Without the IRC damping controller, the maximum tracking bandwidth is reduced to 956 Hz ($k_i = 12000$) with a gain margin of only 2.7 dB. Thus, by using a damping controller, the tracking bandwidth and gain margin are successfully increased by a factor of 2 and 2.7 respectively.

The closed-loop time-domain performance was evaluated by driving the nanopositioner with a full-range (200 V) triangle wave. The open- and closed-loop response is plotted in Fig. 8. At 78 Hz line-rate, the non-linearity is effectively suppressed with negligible tracking lag. Good tracking performance was observed up to around ten-percent of the bandwidth, or approximately 180 Hz.

V. OPEN- AND CLOSED-LOOP PERFORMANCES

To demonstrate the efficacy of the proposed control strategy, this section presents the open- and closed-loop tracking performances of the nanopositioning stage. Fig. 8 plots the measured open- and closed-loop displacements of the nanopositioning stage when the stage was forced to trace triangular inputs at 40 Hz and 78 Hz.

In open-loop, the hysteresis effect of the piezoelectric stack actuator is minimized by the charge drive but not

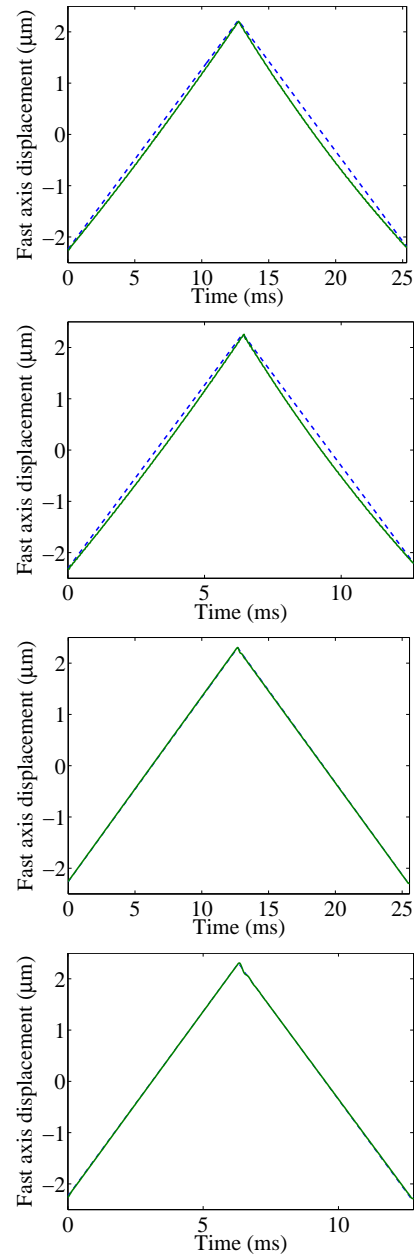


Figure 8. Open-loop tracking performances at 40 Hz (a) and 78 Hz (b). Closed-loop tracking performances at 40 Hz (c) and 78 Hz (d). Reference signals are plotted in dotted-line and displacement measurements are plotted in solid-line.

completely eliminated. The remnant non-linearity is noticeable in the measured displacement plot. The measured closed-loop displacements show significant improvement due to the elimination of non-linearity. With the high tracking bandwidth achieved by the proposed control strategy, the closed-loop system does not exhibit tracking-lag while following a 78-Hz triangular reference.

VI. CONCLUSIONS

In this paper, a piezoelectric strain sensor was bonded to a flexure-based nanopositioner as a displacement sensor for

damping and tracking control. Compared to existing sensors, such as capacitive sensors, piezoelectric strain sensors are extremely low-cost, simple, compact, have a very high bandwidth, and produce low-noise at high frequencies. However, they also exhibit a high-pass characteristic at low frequencies which precludes their use in a tracking control system.

In this work, problems associated with the high-pass characteristic of a piezoelectric sensor are eliminated by using a pair of complementary filters to replace the piezoelectric signal at low frequencies with a displacement estimate based on the present input and open-loop model.

An analog IRC damping controller was designed and implemented to suppress the first resonance mode of the nanopositioner. With damping and integral tracking control, a closed-loop bandwidth of 1.86 kHz was achieved.

The closed-loop tracking performance of the nanopositioning stage was evaluated by forcing the system to track 40-Hz and 78-Hz triangular inputs. The measured closed-loop signals are free from artefacts caused by the nanopositioner non-linearity, even at 78-Hz. These experimental results demonstrate the efficacy of using a piezoelectric strain sensor for damping and tracking control of high-speed nanopositioners.

ACKNOWLEDGMENTS

This research was partly supported by the University of Newcastle Special Project Grant and in part by the Australia Research Council. The research was performed at the Laboratory for Dynamics and Control of Nanosystems at the University of Newcastle.

REFERENCES

- [1] N. Jalili and K. Laxminarayana, "A review of atomic force microscopy imaging systems: application to molecular metrology and biological sciences," *Mechatronics*, vol. 14, no. 8, pp. 907–945, 2004.
- [2] R. A. Oliver, "Advances in AFM for the electrical characterization of semiconductors," *Reports on Progress in Physics*, vol. 71, no. 7, p. 076501, 2008.
- [3] F. Krohs, C. Onal, M. Sitti, and S. Fatikow, "Towards automated nanoassembly with the atomic force microscope: A versatile drift compensation procedure," *Journal of Dynamic Systems, Measurement, and Control*, vol. 131, no. 6, p. 061106, 2009.
- [4] G. Binnig and D. P. E. Smith, "Single-tube three-dimensional scanner for scanning tunneling microscopy," *Review of Scientific Instruments*, vol. 57, no. 8, pp. 1688–1689, 1986.
- [5] T. Ando, T. Uchihashi, N. Kodera, D. Yamamoto, A. Miyagi, M. Taniguchi, and H. Yamashita, "High-speed AFM and nano-visualization of biomolecular processes," *Pflügers Archiv European Journal of Physiology*, vol. 456, no. 1, pp. 211–225, 2008.
- [6] G. Schitter, K. J. Åstrom, B. DeMartini, P. J. Thurner, K. L. Turner, and P. K. Hansma, "Design and modeling of a high-speed AFM-scanner," *IEEE Transactions on Control Systems Technology*, vol. 15, no. 5, pp. 906–915, 2007.
- [7] B. J. Kenton and K. Leang, "Design, characterization, and control of a monolithic three-axis high-bandwidth nanopositioning stage," in *American Control Conference, Baltimore, MD, USA*, 2010.
- [8] Y. K. Yong, S. Aphale, and S. O. R. Moheimani, "Design, identification and control of a flexure-based XY stage for fast nanoscale positioning," *IEEE Transactions on Nanotechnology*, vol. 8, no. 1, pp. 46–54, 2009.
- [9] Y. K. Yong and S. O. R. Moheimani, "A compact XYZ scanner for fast atomic force microscopy in constant force contact mode," in *Proc. IEEE/ASME International Conference on Advanced Intelligent Mechatronics*, Montreal, Canada, July 6-9 2010.
- [10] S. Salapaka, A. Sebastian, J. P. Cleveland, and M. V. Salapaka, "High bandwidth nano-positioner: A robust control approach," *Review of Scientific Instruments*, vol. 73, no. 9, pp. 3232–3241, 2002.
- [11] Y. K. Yong, K. Liu, and S. O. R. Moheimani, "Reducing cross-coupling in a compliant XY nanopositioning stage for fast and accurate raster scanning," *IEEE Transactions on Control Systems Technology*, vol. 18, no. 5, pp. 1172–1179, 2010.
- [12] A. J. Fleming, A. Wills, and S. O. R. Moheimani, "Sensor fusion for improved control of piezoelectric tube scanners," *IEEE Transactions on Control Systems Technology*, vol. 16, no. 6, pp. 1265–1276, November 2008.
- [13] A. J. Fleming, "Nanopositioning system with force feedback for high-performance tracking and vibration control," *IEEE Transactions on Mechatronics*, vol. 15, no. 3, pp. 433–447, June 2010.
- [14] J. L. Fanson and T. K. Caughey, "Positive position feedback control for large space structures," *AIAA Journal*, vol. 28, no. 4, pp. 717 – 724, 1990.
- [15] J. J. Dosch, D. J. Inman, and E. Garcia, "A Self-Sensing Piezoelectric Actuator for Collocated Control," *Journal of Intelligent Material Systems and Structures*, vol. 3, no. 1, pp. 166–185, 1992.
- [16] S. M. Devasia, T. Meressi, B. Panden, and E. Bayo, "Piezoelectric actuator design for vibration suppression-placement and sizing," *Journal of Guidance, Control, and Dynamics*, vol. 16, no. 5, pp. 859–864, 1993.
- [17] Y. Shen and A. Homaifar, "Vibration Control of Flexible Structures with PZT Sensors and Actuators," *Journal of Vibration and Control*, vol. 7, no. 3, pp. 417–451, 2001.
- [18] T. N. Trajkov, H. Koppe, and U. Gabbert, "Vibration control of a funnel-shaped shell structure with distributed piezoelectric actuators and sensors," *Smart Materials and Structures*, vol. 15, no. 4, p. 1119, 2006.
- [19] K. R. Kumar and S. Narayanan, "Active vibration control of beams with optimal placement of piezoelectric sensor/actuator pairs," *Smart Materials and Structures*, vol. 17, no. 5, p. 055008, 2008.
- [20] S. S. Aphale, A. J. Fleming, and S. O. R. Moheimani, "Integral resonant control of collocated smart structures," *Smart Materials and Structures*, vol. 16, pp. 439–446, 2007.
- [21] B. Bhikkaji and S. O. R. Moheimani, "Integral resonant control of a piezoelectric tube actuator for fast nano-scale positioning," *IEEE/ASME Transactions on Mechatronics*, vol. 13, no. 5, pp. 530–537, October 2008.
- [22] J. E. Shigley and C. R. Mischke, *Mechanical Engineering Design*. McGraw-Hill, 1989.
- [23] J. Sirohi and I. Chopra, "Fundamental understanding of piezoelectric strain sensors," *Journal of Intelligent Material Systems and Structures*, vol. 11, no. 4, pp. 246–257, 2000.
- [24] T. McKelvey, H. Akcay, and L. Ljung, "Subspace based multivariable system identification from frequency response data," *IEEE Trans. on Automatic Control*, vol. 41, no. 7, pp. 960–978, July 1996.
- [25] A. J. Fleming, S. Aphale, and S. O. R. Moheimani, "A new method for robust damping and tracking control of scanning probe microscope positioning stages," *IEEE Transactions on Nanotechnology*, vol. 9, no. 4, pp. 438–448, July 2010.
- [26] A. J. Fleming and K. K. Leang, "Charge drives for scanning probe microscope positioning stages," *Ultramicroscopy*, vol. 108, no. 12, pp. 1551–1557, November 2008.
- [27] D. Croft, G. Shedd, and S. Devasia, "Creep, hysteresis, and vibration compensation for piezoactuators: Atomic force microscopy application," *Journal of Dynamic Systems, Measurement, and Control*, vol. 123, no. 1, pp. 35–43, 2001.
- [28] B. Mokaberli and A. A. G. Requicha, "Compensation of scanner creep and hysteresis for AFM nanomanipulation," *IEEE Trans. on Automation Science and Engineering*, vol. 5, no. 2, pp. 197–206, April 2008.
- [29] M. Goldfarb and N. Celanovic, "A lumped parameter electromechanical model for describing the nonlinear behavior of piezoelectric actuators," *Journal of Dynamic Systems, Measurement, and Control*, vol. 119, no. 3, pp. 478–485, 1997.